Available online at www.sciencedirect.com
SCIENCE DIRECT®
Sensors and Actuators B 109 (2005) 19–23
SENSORS AND ACTUATORS B CHEMICAL
www.elsevier.com/locate/snb

Surface oxidation state of combustion-synthesized γ-Fe_2O_3 nanoparticles determined by electron energy loss spectroscopy in the transmission electron microscope

J. Jasinski[a], K.E. Pinkerton[b], I.M. Kennedy[c], V.J. Leppert[a,*]

[a] School of Engineering, University of California, P.O. Box 2039, Merced, CA 95344, USA
[b] Center for Health and the Environment, University of California, Davis, CA 95616, USA
[c] Department of Mechanical and Aeronautical Engineering, University of California, Davis, CA 95616, USA

Available online 1 July 2005

Abstract

Electron energy loss spectroscopy (EELS) in the transmission electron microscope (TEM) was used to compare the iron oxidation state at the surface and interior of γ-Fe_2O_3 nanoparticles produced by the combustion process under fuel conditions leading to low and high soot concentrations. These experiments were performed in the nanoprobe mode, which allowed for very high spatial resolution (the probe size was 1.4 nm). Here, low soot concentrations were obtained in a laminar ethylene–air diffusion flame seeded with iron pentacarbonyl, while high soot concentrations were achieved with the addition of acetylene to this fuel mixture. The studies showed that the surface oxidation state of iron was lowered with the addition of acetylene, although the core composition remained the same. This was indicated by changes in both the iron L_{23}- and the oxygen K-edges at the surface of the particles. These highly spatially-resolved measurements showed a chemical shift of both the L_3 and L_2 iron lines, accompanied by significant reduction of the L_3:L_2-intensity ratio, indicating Fe^{2+} at the particle surface. Reduction in the pre-edge peak of the oxygen K-edge at the particle surface also indicated iron reduction at the surface. These results suggest that the surface oxidation state, and therefore gas-sensing properties, of combustion-synthesized iron oxide nanoparticles is highly dependent on flame conditions. Furthermore, this study shows that EELS is an important research tool for the investigation of nanoscale gas-sensors, allowing differentiation of composition and oxidation state at the interior and surface of individual nanostructures in these materials.

Keywords: Iron oxide; Gas-sensing; EELS; White lines; Oxidation state

1. Introduction

In recent years, semiconducting metal oxides have attracted substantial attention as promising inexpensive gas-sensing materials. Some of the most extensively studied for sensing applications are: titanium oxide (TiO_2) [1–6], indium oxide (In_2O_3) [7–12], gallium oxide (Ga_2O_3) [13–20], and especially tin oxide (SnO_2) [5,19,21–27]. A number of studies have also focused on iron oxide (Fe_2O_3), which, especially in the gamma, cubic phase, exhibits good sensing characteristics towards hydrocarbon gases and carbon monoxide [28–34]. The sensitivity of iron oxide-based sensors can be enhanced by various doping schemes and a number of different dopants such as Pd [29], Sn [35–37], Ti [37], Zn [38,39], etc. While doping is an important factor for controlling the sensing characteristics, the sensor structure, and especially the thickness of its active layer, also has a great influence on the sensitivity. In fact, bulk and thick-film type sensors exhibit a relatively low sensitivity, which substantially improves when the same sensing material is used in a thin-film type sensor. The improvement is even greater when a nanosized material is used. Indeed, experimental studies of sensors produced from SnO_2 nanopowders have shown a systematic increase in sensitivity with decrease in grain size. This increase becomes very drastic when the grain size approaches the double Debye length for electrons, i.e. where the total depletion from carriers is expected to occur within

* Corresponding author.
E-mail address: vleppert@ucmerced.edu (V.J. Leppert).

0925-4005/$ – see front matter © 2005 Elsevier B.V. All rights reserved.
doi:10.1016/j.snb.2005.03.013

grains [40,41]. The increase of sensitivity can also be simply explained by the fact that by reducing the grain/particle size to the nanometer range, its surface-to-bulk ratio greatly increases and it is the metal oxide surface where the gas-sensing takes place. Therefore, there is an increasing interest in using nanosized metal oxides for gas-sensing applications [1,23,42–45].

Various methods have been used to produced nanosized iron oxide powders, including chemical co-precipitation [46,47], sol–gel processes [33,43], spray pyrolysis [45], plasma enhanced chemical vapor deposition [48], and laser ablation [49,50]. Here, in this work, we studied iron oxide nanoparticles prepared by a combustion method under conditions of high and low soot formation. Energy electron loss spectroscopy (EELS) at high spatial resolution was used to study the chemical composition of these particles with the emphasis placed on detecting any changes at the particle surface, since such changes can modify gas-sensing properties of the nanopowder material. Results of this study are discussed in relation to the gas-sensing mechanism of iron oxide-based sensors. Discussion of the impact of surface chemistry and particle morphology on the respiratory toxicity of these materials may be found in ref. [51].

2. Experimental

Iron oxide nanoparticles with sizes ranging from 10 to 40 nm used for this study were produced in a laminar diffusion flame under conditions of low and high soot formation. Under conditions producing a low soot concentration, a laminar ethylene–air diffusion seeded with iron pentacarbonyl was used, while high soot concentrations were achieved with the addition of acetylene to this fuel mixture. In both cases, particles were collected on holey carbon-coated, copper mesh grids using an electrostatic precipitator, for examination in the transmission electron microscope (TEM) and characterization by electron energy loss spectroscopy (EELS). Nanoparticles from the high-soot sample are referred to here as group A. The TEM study of these particles shows that they are embedded in carbonaceous soot and have a tendency to form big clusters (Fig. 1A). Nanoparticles from the low-soot sample are referred to here as group B, have much less or no soot around them, and they are either completely isolated from each other or form small clusters composed usually of only two particles (Fig. 1B).

EELS studies of these nanopowders were performed using a 200 kV CM200 Philips microscope with a field emission gun (producing a beam of energy spread 0.85 eV at HWFM). EELS measurements were carried out in the scanning transmission electron microscopy mode and the smallest possible probe size of 1.4 nm was applied. EELS spectra with a dispersion of 0.3 eV were collected using a Gatan Image Filter (with energy resolution of ~0.9 eV). Both the oxygen K- and the iron L_{23}-EELS ionization edges were acquired. Short acquisition times (5 s) were chosen to minimize undesired

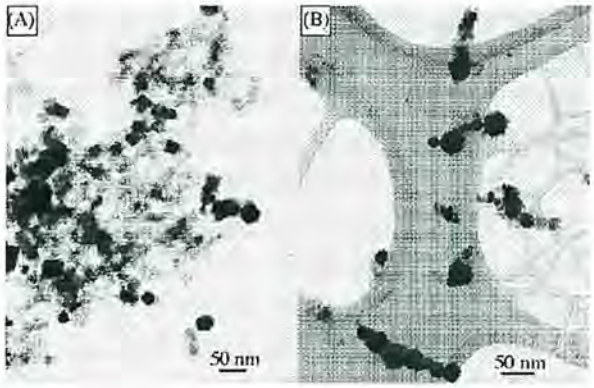

Fig. 1. TEM micrographs of particles from (A) group A and (B) group B.

drift-related effects (substantial reduction in spatial resolution, etc.). Since measurements were carried out in the nanoprobe mode with the smallest probe, such short acquisition times significantly reduced the signal-to-noise ratio in the recorded EELS spectra. Therefore, in order to improve it, which was especially important for spectrum quantification, spectra recorded from several particles were added together and the resulting spectrum was analyzed and quantified. Details of the quantification methods used in this study are the subject of a separate publication [52] and they are only briefly described in the following paragraph.

The L_3:L_2 intensity ratio of the iron L-white lines was quantified in order to determine the iron oxidation state. The standard technique of background removal by fitting a power law formula below the ionization edge was applied [53]. The contribution to the iron L_{23}-ionization edge, originating from the transitions to the continuum of states, was then removed under each L-line using Pearson's method [54] and the intensity of each line was quantified by fitting two Gaussian functions (in order to account for the line asymmetry). Commercially available pure phase nanopowders of several phases of iron oxide were used for calibration. Results obtained for standards were consistent with the L_3:L_2 intensity ratios of iron oxide phases reported by Colliex et al. [55] Therefore, we used the values from their paper as reference for phase identification in nanoparticles produced in the combustion process.

3. Results

EELS measurements show a difference between the two groups of iron oxide nanoparticles. It was found that almost all particles from group A (i.e. particles embedded in the soot) show systematic, very similar differences between their bulk and surface properties. Spectra collected from such particles (obtained after averaging of spectra from 10 nanoparticles), measured at the particle center and at its edge, are shown in Fig. 2. There is a clear difference in the fine structure of the oxygen K-edge between these two spectra. Namely,

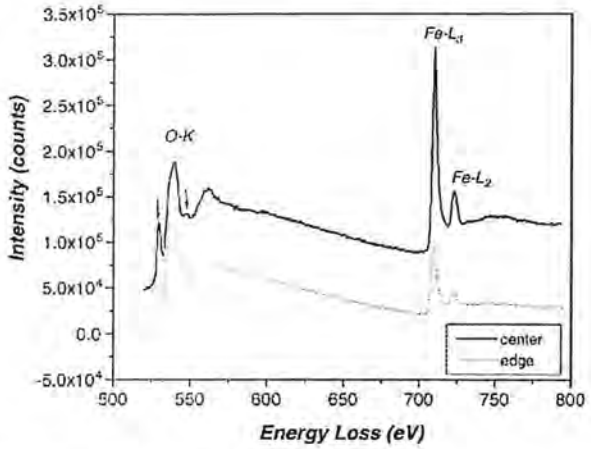

Fig. 2. EELS spectra of the oxygen K- and iron L_{23}-ionization edges measured in the center and at the surface of iron oxide nanoparticles from group A (spectra shown here were obtained by adding data from 10 nanoparticles). Spectra are offset for clarity. Arrows show two features of the O- K-edge typical for γ-Fe_2O_3.

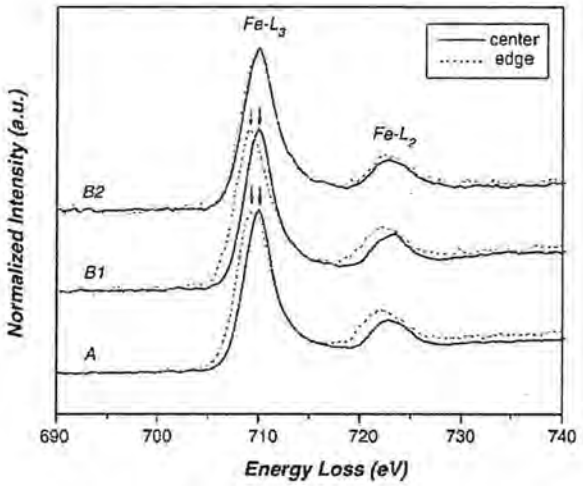

Fig. 3. Normalized EELS spectra of the iron L_{23}-ionization edge measured in the center and at the surface of particles from all three groups. Spectra were offset for clarity. Arrows indicate chemical shift between spectra measured in the center and at the surface.

there are much higher intensities of: (1) the pre-edge peak at ~530 eV and (2) the peak at around 545–500 eV (shown by arrows in Fig. 2) in the spectrum measured at the particle center. Substantial differences are also present in the iron L_{23}-ionization edge, which was evident when the quantification of the iron L-lines was performed. This quantification showed that the L_3:L_2-intensity ratio in the center of such a particle is about 5.5 ± 0.3 compared to about 4.4 ± 0.4 at the surface (Table 1). In addition, the separation between the L_2- and L_3-lines remains constant (about 13 eV), but a significant chemical shift of about 0.6 ± 0.3 eV was detected between these two spectra. This also can be seen from Fig. 3, where normalized EELS spectra of the iron L_{23}-ionization edges measured in the center and at the surface of such particles are shown. These observations are consistent with the findings of Wallis et al. [56] who showed a similar reduced layer on iron oxide particles.

In the case of nanoparticles from group B, formed under low soot conditions, two different surface chemistries are observed. About 60% of these particles (six out of 10), which will be referred as particles of group B1, have properties remarkably similar to these found for nanoparticles from the A group (see Table 1). The L_3:L_2-intensity ratio of iron white lines is again 5.5 ± 0.3 at the center and is about 4.0 ± 0.3 at the surface. Also the chemical shift of about 0.7 ± 0.3 eV of the iron L_{23}-ionization edge was detected between the edge and the center of such particles (see Fig. 3).

The remaining 40% (four out of 10) of particles of the group B, which will be referred to as particles of the group B2, have different properties. The L_3:L_2-intensity ratio measured for these particles differs only slightly between the center and the edge of the particle (5.2 ± 0.3 versus 4.7 ± 0.3) and there is almost no chemical shift between the iron L_{23}-ionization edges measured in the center and at the surface of such particles (see Table 1 and Fig. 3). In addition, the oxygen K-edge spectra measured in the center and at the edge of these particles are similar.

Table 1
Quantification results for iron L-lines

Nanoparticles	L_3:L_2-intensity ratio		Chemical shift (eV)	
	Center	Edge	L_{3c}–L_{3e}	L_{2c}–L_{2e}
A	5.5 ± 0.3	4.4 ± 0.4	0.5 ± 0.3	0.7 ± 0.4
B1	5.5 ± 0.3	4.0 ± 0.4	0.7 ± 0.3	0.7 ± 0.4
B2	5.2 ± 0.3	4.7 ± 0.4	0.1 ± 0.2	0.2 ± 0.2

4. Discussion

The observed changes in the EELS spectra between the edge and the center of a particle from group A or B1 indicate that the chemistry of such a particle is modified at the surface. Results obtained in the center of such a particle, both the value of the L_3:L_2-intensity ratio, as well as the fine structure of the oxygen K-edge, suggest that the core of the particle is composed of either γ-Fe_2O_3 or Fe_3O_4 [55]. This is consistent with X-ray diffraction and selected area electron diffraction measurements [57,58], which indicate that particles are composed mostly of γ-Fe_2O_3, as well as with previous studies [59], which indicate that γ-Fe_2O_3 is a typical iron oxide product of the combustion process. On the other hand, the surface layer of such a particle is composed of FeO as indicated by the L_3:L_2-intensity ratio of about 4 and by the very weak intensities of the oxygen K-edge features indicated in Fig. 2 [55]. In the case of particles from group B, formed under low soot conditions, only a subset (60%) of the nanoparticles show this lower iron oxidation state at the

nanoparticle surface. The particles that were covered with a substantial layer of soot and were not exposed to an oxidizing environment in the flame would be expected to exhibit the reduced surface layer. On the other hand, iron particles that were covered with a thin layer of soot that burned off readily at the flame tip were exposed to a high temperature-oxidizing environment. This condition led to full oxidation to Fe_2O_3. Variations in the soot layer on particles is expected in view of the fairly broad soot particle size distribution in flames that occurs as a result of aerosol coagulation and growth processes in the inhomogeneous environment of a diffusion flame. This type of flame exhibits large gradients in temperature and concentration that affect the history of particles as they pass from a fuel rich interior to a burn-out or oxidation zone at the flame tip.

The results indicate that while the bulk properties of iron oxide nanoparticles may remain the same under a range of combustion conditions, the surface oxidation state of iron, and therefore the gas-sensing capability of the nanoparticles, is highly dependent on the flame conditions. In the commonly accepted mechanism of γ-Fe_2O_3-based sensors, the surface of the γ-Fe_2O_3-based sensor is reduced to Fe_3O_4 when exposed to a reducing gas atmosphere [60]. Since Fe_3O_4 is much more conducting than the γ-Fe_2O_3, the resistivity of the γ-Fe_2O_3 film decreases during exposure to a reducing gas. Such a process does not require any significant change of the structure since both γ-Fe_2O_3 and Fe_3O_4 have the same spinel type crystal structure and their lattice parameters differ only very slightly.

5. Conclusions

Spatially-resolved EELS measurements were used to study iron oxide nanoparticles produced in a combustion process. The study showed that the oxidation state of iron at the surface of the nanoparticles, and therefore their gas-sensing properties, is highly dependent on the flame conditions (fuel mixture/position in flame). EELS performed in STEM mode is an important spectroscopic and analytical technique, capable of studying at a very high spatial resolution the oxidation state and composition at the cores and surfaces of nanosized materials. This technique provides additional information relevant to gas-sensing properties, normally not accessible with bulk characterization techniques, and further insight into the gas-sensing mechanism in these materials.

Acknowledgements

The authors thank Dale Uyeminami for the operation of the diffusion flame system. This research was supported by National Science Foundation grant 0137922, and the National Center for Electron Microscopy at Lawrence Berkeley National Laboratory under U.S. Department of Energy contract DE-AC-03-76SF00098.

References

[1] E. Comini, V. Guidi, C. Frigeri, I. Ricco, G. Sberveglieri, Sens. Actuators B-Chem. 77 (2001) 16–21.
[2] R.M. Geatches, A.V. Chadwick, J.D. Wright, Sens. Actuators B-Chem. 4 (1991) 467–472.
[3] E.E. Gutman, S.V. Ryabtsev, E.A. Kazachkov, M.V. Gerasimov, Sens. Actuators B-Chem. 16 (1993) 338–343.
[4] K.S. Patel, H.T. Sun, Porous Ceramic Materials, vol. 115, 1996, pp. 181–190.
[5] Y. Shimizu, T. Hyodo, M. Egashira, Catal. Surveys Asia 8 (2004) 127–135.
[6] E. Traversa, G. Gnappi, A. Montenero, G. Gusmano, Sens. Actuators B-Chem. 31 (1996) 59–70.
[7] T. Skala, K. Veltruska, M. Moroseac, I. Matolinova, G. Korotchenkov, V. Matolin, Appl. Surf. Sci. 205 (2003) 196–205.
[8] T.K.H. Starke, G.S.V. Coles, H. Ferkel, Sens. Actuators B-Chem. 85 (2002) 239–245.
[9] V. Marotta, S. Orlando, G.P. Parisi, A. Giardini, G. Perna, A.M. Santoro, V. Capozzi, Appl. Surf. Sci. 168 (2000) 141–145.
[10] D. Sauter, U. Weimar, G. Noetzel, J. Mitrovics, W. Gopel, Sens. Actuators B-Chem. 69 (2000) 1–9.
[11] F. Quaranta, R. Rella, R. Siciliano, S. Capone, C. Distante, M. Epifani, A. Taurino, Sens. Actuators B-Chem. 84 (2002) 55–59.
[12] A.A. Tomchenko, G.P. Harmer, B.T. Marquis, J.W. Allen, Sens. Actuators B-Chem. 93 (2003) 126–134.
[13] J. Giber, I.V. Perczel, J. Gerblinger, U. Lampe, M. Fleischer, Sens. Actuators B-Chem. 18 (1994) 113–118.
[14] J. Frank, M. Fleischer, H. Meixner, Sens. Actuators B-Chem. 34 (1996) 373–377.
[15] J. Frank, M. Fleischer, H. Meixner, A. Feltz, Sens. Actuators B-Chem. 49 (1998) 110–114.
[16] J. Frank, M. Fleischer, H. Meixner, Sens. Actuators B-Chem. 48 (1998) 318–321.
[17] T. Schwebel, M. Fleischer, H. Meixner, C.D. Kohl, Sens. Actuators B-Chem. 49 (1998) 46–51.
[18] R. Pohle, M. Fleischer, H. Meixner, Sens. Actuators B-Chem. 68 (2000) 151–156.
[19] U. Hoefer, J. Frank, M. Fleischer, Sens. Actuators B-Chem. 78 (2001) 6–11.
[20] G. Kiss, Z. Pinter, I.V. Perczel, Z. Sassi, F. Reti, Thin Solid Films 391 (2001) 216–223.
[21] A. Nakajima, J. Mater. Sci. Lett. 12 (1993) 1778–1780.
[22] S.L. Sharp, G. Kumar, E.P. Vicenzi, A.B. Bocarsly, M. Heibel, Chem. Mater. 10 (1998) 880–885.
[23] J. Puigcorbe, A. Cirera, J. Cerda, J. Folch, A. Cornet, J.R. Morante, Sens. Actuators B-Chem. 84 (2002) 60–65.
[24] C. Pijolat, B. Riviere, M. Kamionka, J.P. Viricelle, P. Breuil, J. Mater. Sci. 38 (2003) 4333–4346.
[25] A. Tiburcio-Silver, A. Sanchez-Juarez, Mater. Sci. Eng. B-Solid State Mater. Adv. Technol. 110 (2004) 268–271.
[26] N. Barsan, U. Weimar, J. Phys.-Condensed Matter 15 (2003) R813–R839.
[27] N. Barsan, M. Schweizer-Berberich, W. Gopel, Fres. J. Anal. Chem. 365 (1999) 287–304.
[28] Y. Nakatani, M. Matsuoka, Y. Iida, Am. Ceram. Soc. Bull. 60 (1981) 401.
[29] D.-D. Lee, D.-H. Choi, Sens. Actuators B-Chem. 1 (1990) 231–235.
[30] J. Peng, C.C. Chai, Sens. Actuators B-Chem. 14 (1993) 591–593.
[31] Z. Tianshu, L. Hongmei, Z. Huanxing, Z. Ruifang, S. Yusheng, Sens. Actuators B-Chem. 32 (1996) 181–184.
[32] K. Siroky, J. Jiresova, L. Hudec, Thin Solid Films 245 (1994) 211–214.
[33] S.W. Tao, X.Q. Liu, X.F. Chu, Y.S. Shen, Sens. Actuators B-Chem. 61 (1999) 33–38.
[34] I.S. Lim, G.E. Jang, C.K. Kim, D.H. Yoon, Sens. Actuators B-Chem. 77 (2001) 215–220.

[35] H. Kanai, H. Mizutani, T. Tanaka, T. Funabiki, S. Yoshida, M. Takano, J. Mater. Chem. 2 (1992) 703–707.
[36] C.V.G. Reddy, W. Cao, O.K. Tan, W. Zhu, Sens. Actuators B-Chem. 81 (2002) 170–175.
[37] O.K. Tan, W. Cao, W. Zhu, J.W. Chai, J.S. Pan, Sens. Actuators B-Chem. 93 (2003) 396–401.
[38] G. Neri, A. Bonavita, S. Galvagno, P. Siciliano, S. Capone, Sens. Actuators B-Chem. 82 (2002) 40–47.
[39] A.A. Vasiliev, M.A. Polykarpov, Sens. Actuators B-Chem. 7 (1992) 626–629.
[40] C. Xu, J. Tamaki, N. Miura, N. Yamazoe, Sens. Actuators B-Chem. 3 (1991) 147–155.
[41] N. Yamazoe, Sens. Actuators B-Chem. 5 (1991) 7–19.
[42] M.I. Baraton, L. Merhari, Nanostruct. Mater. 10 (1998) 699–713.
[43] L.J. Ma, T. Yan, S.L. Bai, X.W. Huang, Y.J. Song, A.F. Chen, C.C. Liu, Chin. J. Chem. Eng. 12 (2004) 282–285.
[44] K. Suri, S. Annapoorni, A.K. Sarkar, R.P. Tandon, Sens. Actuators B-Chem. 81 (2002) 277–282.
[45] S.Y. Wang, W. Wang, W.Z. Wang, Z. Jiao, J.H. Liu, Y.T. Qian, Sens. Actuators B-Chem. 69 (2000) 22–27.
[46] W.Y. Chung, D.D. Lee, Thin Solid Films 200 (1991) 329–339.
[47] X.T. Ge, X.Q. Liu, Acta Phys.-Chim. Sinica 17 (2001) 887–891.
[48] Y. Liu, W. Zhu, O.K. Tan, Y. Shen, Mater. Sci. Eng. B-Solid State Mater. Adv. Technol. 47 (1997) 171–176.
[49] S.R. Shinde, A.G. Banpurkar, K.P. Adhi, A.V. Limaye, S.B. Ogale, S.K. Date, G. Marest, Mod. Phys. Lett. B 10 (1996) 1517–1527.
[50] X. Zeng, N. Koshizaki, T. Sasaki, Appl. Phys. Mater. Sci. Process. 69 (1999) S253–S255.
[51] V.J. Leppert, K.E. Pinkerton, J. Jasinski, in: David C. Martin, David A. Muller, Paul A. Midgley, Eric A. Stach (Eds.), Materials Research Society Symposium Proceedings 839, Warrendale, PA, 2005, P2.7.1.
[52] J. Jasinski, K.E. Pinkerton, V.J. Leppert, Microsc. Microanal., submitted for publication.
[53] R.F. Egerton, Electron Energy Loss Spectroscopy in the Electron Microscope, 2nd ed., Plenum Press, New York and London, 1996.
[54] D.H. Pearson, B. Fultz, C.C. Ahn, Appl. Phys. Lett. 53 (1988) 1405–1407.
[55] C. Colliex, T. Manoubi, C. Ortiz, Phys. Rev. B 44 (1991) 11402–11411.
[56] D.J. Wallis, N.D. Browning, C.M. Megaridis, P.D. Nellist, J. Microsc. 184 (1996) 185–194.
[57] K.E. Pinkerton, Y.-M. Zhou, S.V. Teague, J.L. Peake, R.C. Walther, I.M. Kennedy, V.J. Leppert, A.E. Aust, Inhal. Toxicol. 16 (2004) 73–81.
[58] Y.-M. Zhou, C.-Y. Zhong, I.M. Kennedy, V.J. Leppert, K.E. Pinkerton, Toxicol. Appl. Pharmacol. 190 (2003) 157.
[59] C. Janzen, P. Roth, Combus. Flame 125 (2001) 1150–1161.
[60] M. Fujinami, Y. Ujihira, J. Mater. Sci. 20 (1985) 1859–1863.

Biographies

Jacek Jasinski is a Researcher in the School of Engineering at UC Merced. He studies the chemistry and structure of oxide and semiconductor nanoparticulates and thin films using advanced techniques in transmission electron microscopy. His current work focuses on the use of monochromated electron energy-loss spectroscopy and in situ experiments in characterizing nanoparticles for device applications.

Kent Pinkerton is Professor and Director of the Center for Health and the Environment at the University of California, Davis. His research efforts focus on issues critical to environmental air pollution and their impact on the respiratory system.

Ian Kennedy is Professor of Mechanical and Aeronautical Engineering at the University of California, Davis. His research interests are ultra-fine particles and their effects on health; the formation of nanoparticles and their characteristics; applications of nanoparticles in biosensors.

Valerie Leppert is Assistant Professor and a founding faculty member in the School of Engineering at the University of California, Merced. Her research interest is the characterization of technological and environmental nanomaterials in the transmission electron microscope, particularly the application of new microscopy techniques to the study of these materials.